

A Comparison of SIR-B Synthetic Aperture Radar Data with Ocean Internal Wave Measurements

R. F. GASPAROVIC, J. R. APEL, D. R. THOMPSON, J. S. TOCHKO

An image from the Shuttle Imaging Radar-B (SIR-B) synthetic aperture radar (SAR) shows internal wave features in an area south of Long Island, New York. Coincident oceanographic measurements are used in conjunction with hydrodynamic interaction and electromagnetic scattering models to estimate the expected SAR image intensity modulations associated with the internal waves. There is reasonable agreement between the predicted and observed internal wave signatures.

DURING ORBIT 96 (11 OCTOBER 1984) of the Shuttle Imaging Radar-B (SIR-B) mission on the space shuttle Challenger, a synthetic aperture radar (SAR) image of oceanic internal waves was obtained simultaneously with ship and current-meter measurements of the waves. These observations were part of the second phase of the Synthetic Aperture Radar Signature Experiment (SARSEX), a major experiment sponsored by the Office of Naval Research to investigate the basic hydrodynamic and electromagnetic phenomena responsible for internal wave signatures in SAR images and to test theories for predicting such signatures. The SIR-B image taken at 05:03:08 EDT (Fig. 1) shows several packets of tidally generated internal waves, low to moderate wind fronts, and the location of the research vessel *Cape*. The geographical area extends from about 100 km south of Long Island to immediately northeast of the Hudson Canyon, near 40°N, 72°15'W, a region that had been studied by Apel and co-workers (1, 2) during observational programs on internal waves on the continental shelf.

In situ measurements were made of horizontal water velocity components from current meters at depths of 15 and 67 m, water column temperature and density profiles, 200-kHz downward-looking echo sounder internal wave profiles, surface wave height spectra, and wind speed. The major properties of the internal wave field can be estimated when these measurements are used in conjunction with an internal wave model. For example, the lead wave seen at the location of R.V. *Cape* in Fig. 1 is moderately well fitted by a wave profile of the form

$$\eta = \eta_0 \cos^2[K(x - ct)] \quad (1)$$

which describes the amplitude η of an internal wave of wave number K and wavelength $L = 2\pi/K$ propagating at a phase speed c .

From the in situ measurements and a solution of the internal wave equation (3), we find that $\eta_0 \approx 9$ m, $L \approx 250$ m, and $c \approx 0.4$ m sec⁻¹. At the surface the estimated maximum induced current $u_0 \approx 0.15$ m sec⁻¹, and the maximum surface current gradient or strain rate is approximately 0.004 sec⁻¹.

A more extensive observational program of some nonlinear internal waves was carried out 4 weeks earlier during phase I of SARSEX. This effort was structured to quantify the dominant processes contributing to the SAR signatures of internal waves: (i) the internal wave hydrodynamics, especially the surface current strain rates; (ii) modifications to the surface wave spectrum induced by the currents; (iii) the radar backscatter from the modulated surface waves; and (iv) the formation of SAR images from the backscatter modulations. Phase I, which involved two research vessels and three aircraft including a Canadian CV-580 aircraft with the ERIM X- and L-band SAR system (4), yielded excellent data on the internal wave signatures in this region. Preliminary results from phase I have been reported (5-7), and intensive analyses are under way.

A theory describing the perturbation of the surface wave height spectrum by the internal wave surface currents (8) has been used to calculate the expected backscatter modulations associated with the internal waves. This theory assumes that the energy input from the wind acts to restore the surface wave height spectrum $S(\mathbf{k}, \mathbf{x}, t)$, which is perturbed by the presence of the internal wave currents $\mathbf{u}(\mathbf{x}, t)$, to its equilibrium value $S_0(\mathbf{k})$. In particular, it is assumed that the fractional change in the wave action spectrum

$$N(\mathbf{k}, \mathbf{x}, t) = \rho \frac{\omega}{k} S(\mathbf{k}, \mathbf{x}, t) \quad (2)$$

(where ρ is the water density) is proportional to the departure of the spectrum from its

equilibrium value $N_0(\mathbf{k})$. Mathematically, this implies

$$\begin{aligned} \frac{1}{N} \frac{dN}{dt} &= \frac{1}{N} \left(\frac{\partial N}{\partial t} + \dot{\mathbf{x}} \cdot \nabla_{\mathbf{x}} N + \dot{\mathbf{k}} \cdot \nabla_{\mathbf{k}} N \right) \\ &= - \frac{\beta(\mathbf{k})}{N_0} (N - N_0) \end{aligned} \quad (3)$$

where

$$\dot{x}_i = \frac{\partial \omega}{\partial k_i} + u_i \quad (4a)$$

and

$$\dot{k}_i = -k_j \frac{\partial u_j}{\partial x_i} \quad (4b)$$

In these equations, ω is the wave frequency, the indices $i, j = 1, 2$ denote horizontal coordinates, and repeated indices are summed. The function $\beta(\mathbf{k})$ —the so-called wave relaxation rate—determines the effectiveness of the wind in restoring equilibrium. There is, at present, considerable uncertainty about its exact functional form, although there is general agreement that it increases with wave number and wind speed. We made the calculations that follow by using Hughes' expression for $\beta(\mathbf{k})$ (8), which is consistent with field observations.

To relate the internal wave-induced change in surface wave spectrum to the SAR image intensity modulation, we make use of the fact that ocean backscatter at the SIR-B radar wavelength $\lambda_0 = 23.5$ cm and incidence angle θ is dominated by Bragg scattering (9). In this limit, the normalized radar cross section σ is proportional to the surface wave spectrum of the Bragg waves, that is, those waves traveling in the radar "look" direction with a wavelength $\lambda_B = \lambda_0/2(\sin \theta)$. The fractional change in cross section from its mean value σ_0 is given by

$$\frac{\Delta\sigma}{\sigma_0} = \frac{N(\mathbf{k}_B, \mathbf{x}, t) - N_0(\mathbf{k}_B)}{N_0(\mathbf{k}_B)} \quad (5)$$

where \mathbf{k}_B is the Bragg wave number. When the internal wave features propagate in the radar look direction as in Fig. 1, the SAR image intensity variations are essentially equivalent to the cross-sectional variations given by Eq. 5.

Image intensity variations for some of the features of the internal waves in Fig. 1 are shown in Fig. 2. Figure 2a, taken through the wave group along the vertical line A-A', shows nine distinct waves in the packet with peak-to-peak intensity variations ranging from 2 to 12 dB. The average spacing between waves in this packet is approximately 380 m. There is another group of waves near the center of the image along the vertical line B-B' (Fig. 2b). The four waves at the front of this packet have peak-to-peak

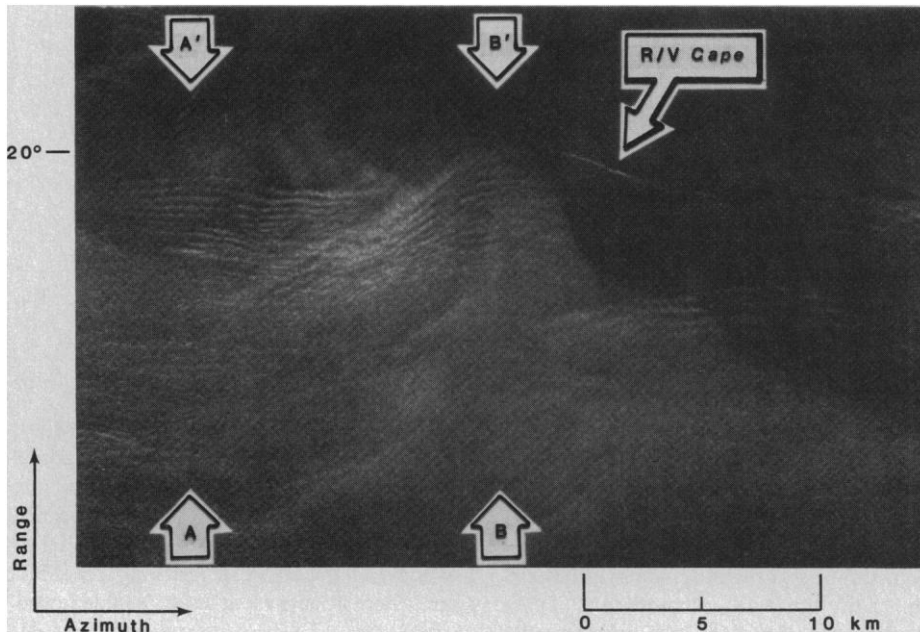


Fig. 1. SAR image of oceanic internal wave features from orbit 96 of the SIR-B mission. The bright linear features crossing lines A-A' and B-B' are due to increased surface wave roughness within the internal wave packets, which are propagating toward the top of the image (313° true heading). A surface wind of 1 m sec⁻¹, blowing toward 190° true heading, was recorded at the ship position. The radar incidence angle at the center of the image is 20°.

intensity variations (along line B-B') of 3 to 10 dB.

We have made predictions of the SAR image intensity modulations for these internal waves, using the above theory with internal wave and surface parameters obtained from the in situ observations. Maximum internal wave surface strain rates of

0.002 to 0.005 sec⁻¹ were assumed, consistent with intrapacket variations encountered during the phase I observations. The large-scale brightness variations in Fig. 1 are indicative of the presence of wind speeds greater than the value 1 m sec⁻¹ recorded at the ship location. For the wave packet along A-A', we assumed a wind speed of 2 m

sec⁻¹; along line B-B', the wind speed is presumed to lie between these two values. With a wind speed of 2 m sec⁻¹, the calculated peak-to-peak SAR image intensity modulations range from 2 to 7 dB for maximum surface strain rates of 0.002 and 0.005 sec⁻¹, respectively. These calculated modulations agree with the observations along lines A-A' and B-B' to within 3 to 5 dB, or within a factor of 2 to 3. This result is consistent with initial findings for the phase I L-band SAR images, for which more extensive comparisons between theory and observations are possible (6, 7).

The single bright feature at the location of R.V. *Cape* appears to belong to the lead wave in the packet along line B-B'. Figure 2c shows the signature from this wave, located just to the left of the position of R.V. *Cape*. In this area of the image there is very little backscatter from the ambient sea because of the low wind speed, and this particular internal wave has apparently generated a significant amount of small-scale surface roughness on an otherwise calm sea, producing the large change (23 dB) in cross section observed in the SAR image. Effects of this type are outside the applicable domain of the above wave-current interaction model in which the backscatter changes arise via current-induced modulations to an existing equilibrium surface wave spectrum. An effort to develop a more appropriate description is planned in conjunction with future analysis of the SARSEX data.

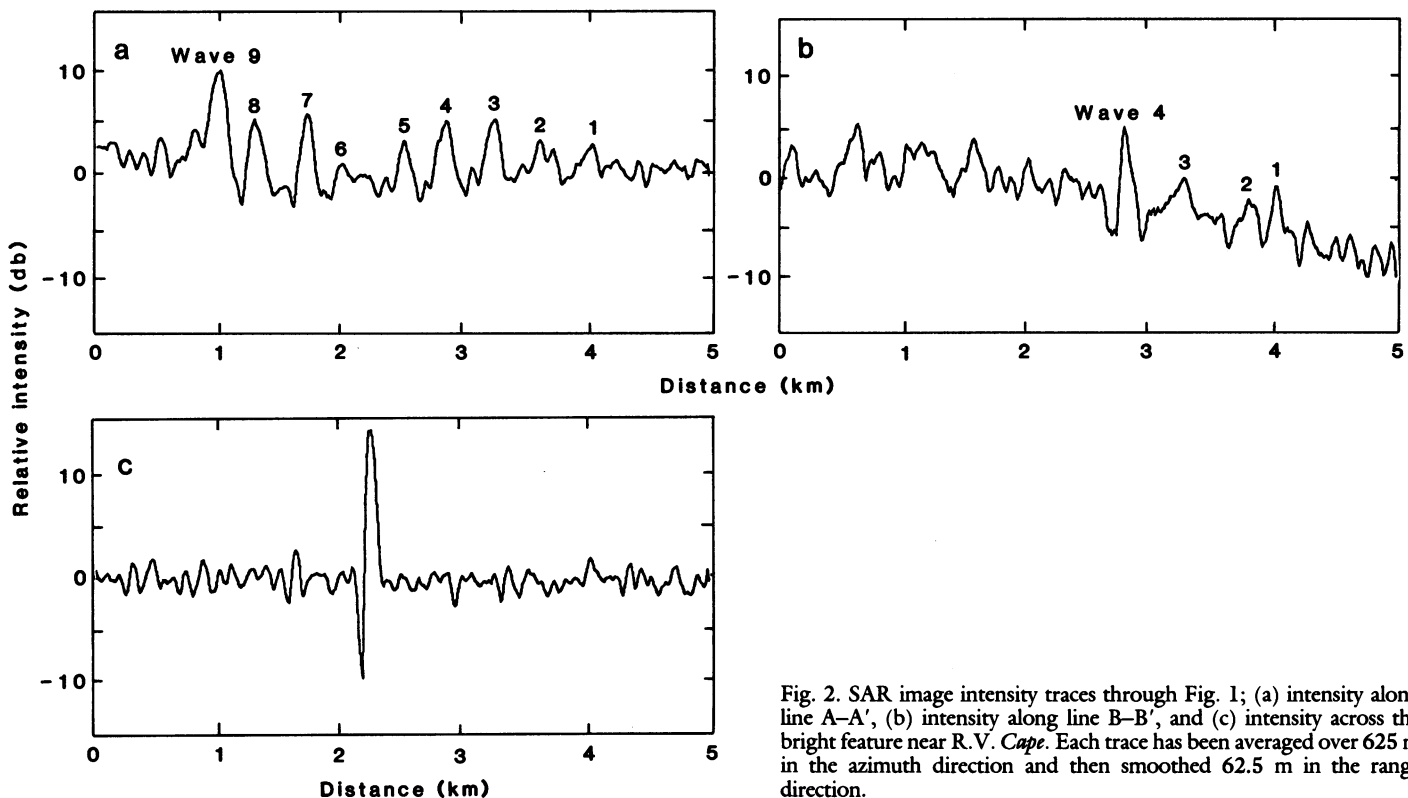


Fig. 2. SAR image intensity traces through Fig. 1; (a) intensity along line A-A', (b) intensity along line B-B', and (c) intensity across the bright feature near R.V. *Cape*. Each trace has been averaged over 625 m in the azimuth direction and then smoothed 62.5 m in the range direction.

A Comparison of SIR-B Directional Ocean Wave Spectra with Aircraft Scanning Radar Spectra

R. C. BEAL, F. M. MONALDO, D. G. TILLEY, D. E. IRVINE, E. J. WALSH, F. C. JACKSON, D. W. HANCOCK III, D. E. HINES, R. N. SWIFT, F. I. GONZALEZ, D. R. LYZENGA, L. F. ZAMBRESKY

Directional ocean wave spectra derived from Shuttle Imaging Radar-B (SIR-B) L-band imagery collected off the coast of southern Chile on 11 and 12 October 1984 were compared with independent spectral estimates from two airborne scanning radars. In sea states with significant wave heights ranging from 3 to 5 meters, the SIR-B-derived spectra at 18° and 25° off nadir yielded reasonable estimates of wavelengths, directions, and spectral shapes for all wave systems encountered, including a purely azimuth-traveling system. A SIR-B image intensity variance spectrum containing predominantly range-traveling waves closely resembles an independent aircraft estimate of the slope variance spectrum. The prediction of a U.S. Navy global spectral ocean wave model on 11 October 1984 exhibited no significant bias in dominant wave number but contained a directional bias of about 30° with respect to the mean of the aircraft and spacecraft estimates.

THE ABILITY TO MAKE ACCURATE global estimates of the directional wave energy spectrum of the ocean has been a goal of oceanographers for at least two decades (1). Such a capability would revolutionize our knowledge of global wave climatology, and the validation, refinement, and periodic updating of existing ocean wave forecast models would immediately become a practical possibility.

Few techniques exist for estimating the directional wave spectrum. Directional wave rider buoys, developed in the 1960's, have been widely utilized and are useful for characterizing unimodal wave systems at a single location. However, with directional buoys it is difficult to measure spectral widths, and such measurements become confused in the presence of bimodal wave systems traveling in different directions. Aircraft stereopho-

tography is sometimes useful, but it is limited by clouds and is not a candidate for a global all-weather operational system.

In 1978, the Seasat synthetic aperture radar (SAR) obtained the first high-resolution radar images of the ocean from space, demonstrating its potential as a global monitoring system for directional energy spectra. However, the SAR-measured ocean backscatter is only indirectly related to the ocean wave height or energy. Moreover, some theoretical models predict that highly non-linear imaging mechanisms can dominate the transformation from SAR backscatter to ocean height (2), contaminating the SAR image to such an extent that inversion to an absolute energy spectrum would become impossible. Although such catastrophic situations have not been observed in any of the published Seasat SAR data, Seasat spectra were affected by azimuth (along-track) filtering, which acted to rotate (and sometimes obliterate) wave systems having a significant azimuth component (3, 4).

The details of the SAR azimuth contamination depend upon the hydrodynamic and electromagnetic properties of the moving sea surface (5); independent of these details, however, the degree of contamination is directly proportional to the range-to-velocity ratio (R/V) of the radar platform. The R/V ratio for Seasat at an altitude of 800 km and an off-nadir angle of 20° was about 130 seconds; R/V for Shuttle Imaging Radar-B (SIR-B) at 230-km altitude and a similar off-nadir angle was only 35 seconds. Therefore, the spectral contamination that was evident in Seasat SAR spectra, whatever its exact cause in terms of scatterer motion, should

Table 1. Summary of estimated and predicted wave systems for 11 and 12 October 1984. Listed are wave number k and direction θ of all detected wave systems along with their associated spectral widths Δk and $\Delta\theta$.

Source	Primary wave system*					Secondary wave system†			
	H_s (m)	k (rad/m)	Δk (rad/m)	θ (deg)	$\Delta\theta$ (deg)	k (rad/m)	Δk (rad/m)	θ (deg)	$\Delta\theta$ (deg)
<i>12 October</i>									
SCR	3.4	0.017	0.008	103	50				
ROWS	3.9	0.017	0.010	98	52	0.047	0.013	204	30
SIR-B‡	3.5	0.019	0.012	97	70	0.048	0.014	205	30
<i>11 October</i>									
ROWS	4.8	0.024	0.013	146	39	0.052	0.012	143	32
SIR-B‡	4.0	0.025	0.012	143	33	0.052	0.014	150	30
GSOWM (55°S)	3.0	0.025	0.023	172	60				
GSOWM (50°S)	4.9	0.023	0.025	135	77				

*Primary wave parameters were estimated from integrated variance spectra, with k, θ centered at about half-power ($\Delta k, \Delta\theta$) points. †Secondary wave parameters were estimated with spectral cuts through the slope spectra. ‡Estimates of H_s for normalizing SIR-B spectra were obtained from an aircraft nadir-looking radar altimeter.

R. C. Beal, F. M. Monaldo, D. G. Tilley, D. E. Irvine, Johns Hopkins University Applied Physics Laboratory, Laurel, MD 20707.

E. J. Walsh, F. C. Jackson, D. W. Hancock III, D. E. Hines, NASA Goddard Space Flight Center, Greenbelt, MD 20771.

R. N. Swift, EG&G Analytical Services Center, Inc., Pocomoke City, MD 21851.

F. I. Gonzalez, National Oceanic and Atmospheric Administration Pacific Marine Environmental Laboratory, Seattle, WA 98115.

D. R. Lyzenga, Environmental Research Institute of Michigan, Ann Arbor, MI 48107.

L. F. Zambresky, Fleet Numerical Oceanography Center, Monterey, CA 93940.